




# Active Sites in Cr(III)-Based Ethylene Polymerization Catalysts from Machine-Learning-Supported XAS and EPR Spectroscopy

## Journal Article

### Author(s):

Ashuiev, Anton ; Nobile, Anna Giorgia ; Trummer, David; Klose, Daniel; Guda, Sergey; Safonova, Olga V.; Copéret, Christophe ; Guda, Alexander; Jeschke, Gunnar

### Publication date:

2024-01-02

### Permanent link:

<https://doi.org/10.3929/ethz-b-000648016>

### Rights / license:

[Creative Commons Attribution-NonCommercial 4.0 International](#)

### Originally published in:

Angewandte Chemie. International Edition 63(1), <https://doi.org/10.1002/anie.202313348>

### Funding acknowledgement:

192050 - Molecular Approach and Understanding in Heterogeneous Catalysis (SNF)  
169134 - Molecular Approach to Heterogeneous Catalysis (SNF)

## Heterogeneous Catalysis

# Active Sites in Cr(III)-Based Ethylene Polymerization Catalysts from Machine-Learning-Supported XAS and EPR Spectroscopy\*\*

Anton Ashuiev<sup>+</sup>, Anna Giorgia Nobile<sup>+</sup>, David Trummer, Daniel Klose, Sergey Guda, Olga V. Safonova, Christophe Copéret,<sup>\*</sup> Alexander Guda,<sup>\*</sup> and Gunnar Jeschke<sup>\*</sup>

**Abstract:** The ethylene polymerization Phillips catalyst has been employed for decades and is central to the polymer industry. While Cr(III) alkyl species are proposed to be the propagating sites, there is so far no direct experimental evidence for such proposal. In this work, by coupling Surface organometallic chemistry, EPR spectroscopy, and machine learning-supported XAS studies, we have studied the electronic structure of well-defined silica-supported Cr(III) alkyls and identified the presence of several surface species in high and low-spin states, associated with different coordination environments. Notably, low-spin Cr(III) sites are shown to participate in ethylene polymerization, indicating that similar Cr(III) alkyl species could be involved in the related Phillips catalyst.

## Introduction

Polyethylene (PE) is still one of the most important products of the chemical industry with a broad range of applications that have changed our modern life. While nearly 50 % of the global polyethylene production is based on Ti-based hetero-

geneous Ziegler–Natta catalysts,<sup>[1]</sup> another 40 % is produced by the Cr-based Phillips catalysts.<sup>[2]</sup> This industrial system was developed in the 1950s by Phillips Petroleum and is prepared by dispersing Cr precursors on silica (SiO<sub>2</sub>), followed by calcination in a flow of dry air or oxygen at elevated temperatures.<sup>[2–3]</sup> This treatment yields isolated Cr(VI) sites that are then reduced upon contact with ethylene during an induction period.<sup>[3]</sup> A vast range of spectroscopic studies of the Phillips catalytic system were performed, often complemented by computational methods.<sup>[3]</sup> Based on Raman,<sup>[4]</sup> UV/Vis,<sup>[5]</sup> EPR,<sup>[6]</sup> and X-ray absorption spectroscopy (XAS)<sup>[7]</sup> techniques, a vast range of surface and active sites structures with different coordination environments and oxidation states (II–IV) have been proposed (see Figure 1, top). This debate highlights the challenge in characterizing this industrial system due to the high heterogeneity and low number of active sites. Recent studies on the Phillips system and related surface-supported Cr silicates, prepared by Surface organometallic chemistry (SOMC), have supported Cr(III) as the active sites.<sup>[7–8]</sup> Noteworthy, the Union Carbide catalyst, an alternative Cr-based ethylene polymerization system, has also been shown to involve Cr(III) hydride and alkyl species as active sites.<sup>[9]</sup> Therefore, Cr(III) alkyl species are reasonable candidates for the active sites of the Phillips catalyst. While the formation of Cr(III) species upon contact with ethylene has been clearly evidenced on the Phillips catalyst with continuous-wave (CW) EPR spectroscopy,<sup>[6]</sup> only a fraction of these

[\*] A. Ashuiev,<sup>+</sup> A. Giorgia Nobile,<sup>+</sup> D. Trummer, D. Klose, C. Copéret, G. Jeschke  
 Department of Chemistry and Applied Biosciences, ETH Zürich  
 Vladimir Prelog Weg 1-5, 8093 Zürich (Switzerland)  
 E-mail: ccoperet@ethz.ch  
 gjeschke@ethz.ch

S. Guda, A. Guda  
 The Smart Materials Research Institute, Southern Federal University  
 Sladkova 178/24, Rostov-on-Don, 344090 (Russia)  
 E-mail: guda@sfnu.ru

O. V. Safonova  
 Paul Scherrer Institut, WLG/217  
 Forschungsstrasse 111, 5232 Villigen PSI (Switzerland)

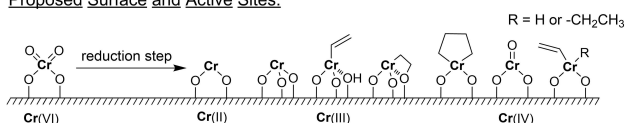
[<sup>+</sup>] These authors contributed equally to this work.

[\*\*] A previous version of this manuscript has been deposited on a preprint server (<https://doi.org/10.26434/chemrxiv-2023-34wl2>).

© 2023 The Authors. Angewandte Chemie International Edition published by Wiley-VCH GmbH. This is an open access article under the terms of the Creative Commons Attribution Non-Commercial License, which permits use, distribution and reproduction in any medium, provided the original work is properly cited and is not used for commercial purposes.

## Phillips catalyst:

### Proposed Surface and Active Sites:



## This work:

### Well-defined Cr(III) Alkyl

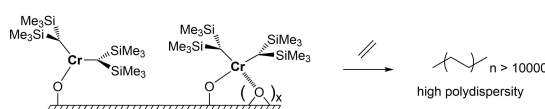


**Figure 1.** Top: Proposed surface and active Cr species in the industrial Phillips catalyst after reduction. Bottom: Well-defined bis alkyl Cr(III) ethylene polymerization sites, studied in the course of the present work.

sites typically participates in ethylene polymerization.<sup>[2,6]</sup> In fact, recent XAS studies of the Phillips system, combined with advanced machine learning (ML) approaches,<sup>[7]</sup> suggest that Cr(III) and Cr(VI) sites in different coordination environments are the major surface components after contact with C<sub>2</sub>H<sub>4</sub>. While highly coordinated Cr(III) silicates are the major fraction (ca. 80 %) of the Cr species, they are most likely not involved in ethylene polymerization. At the same time, low-coordinated Cr(III) alkyl species likely represent only a limited fraction that lies beyond the XAS detection limit and overlap with the spectral signatures of Cr(II) sites.<sup>[7]</sup> The large number of different surface sites whose spectroscopic features are overlapping, as well as the low amount of active species, are therefore the main obstacles preventing the direct observation of the active sites.

This problem can be tackled by preparing and further characterizing related model systems that would result in isolated well-defined silica-supported Cr species while being also active in ethylene polymerization. Similarities with the Phillips catalyst in the produced PE properties, such as molecular weight ( $M_w$ ) and dispersity ( $M_w/M_n$ ), typically suggest analogies regarding the nature of active sites.<sup>[10]</sup> Using these criteria, Monoi et al. prepared the closest system to the Phillips catalysts by contacting the molecular Cr(III) alkyl complex Cr[CH(SiMe<sub>3</sub>)<sub>2</sub>]<sub>3</sub> with pre-calcined silica.<sup>[11]</sup> This material shows high activity for ethylene polymerization without an induction period and does not require cocatalysts, thus suggesting the surface species generated upon grafting are related to the active sites. In addition, this catalyst produces PE with  $M_w$  and  $M_w/M_n$  values close to those obtained from the industrial Phillips catalyst. The temperature dependence of those parameters also appeared akin for both systems,<sup>[11]</sup> further highlighting their similarity. Yet, the detailed structure and the oxidation state of Cr surface sites in Cr[CH(SiMe<sub>3</sub>)<sub>2</sub>]<sub>3</sub>@SiO<sub>2</sub> remain to be ascertained. Recent spectroscopic studies, including CW EPR, have led to postulate the presence of several types of high-spin Cr(III) sites as well as Cr(V) species.<sup>[12]</sup>

Here, aiming at understanding the nature of surface sites in silica-supported Cr[CH(SiMe<sub>3</sub>)<sub>2</sub>]<sub>3</sub>, we have used partially dehydroxylated silica, thermally treated at 700 °C under high vacuum (SiO<sub>2-700</sub>), which contains mostly isolated OH groups and thus yields well-defined mono-grafted surface species, hence simplifying its characterization.<sup>[13]</sup> Using a recently developed supervised ML analysis of XAS data,<sup>[7]</sup> we investigate the oxidation state and local environment of possible surface sites and further refine their structure with the help of EPR spectroscopy. In particular, we show that the major surface species correspond to mono-grafted bis-alkyl Cr(III) complexes, (≡SiO)–Cr[CH((SiMe<sub>3</sub>)<sub>2</sub>)<sub>2</sub>], which are present in both high-spin (HS) and low-spin (LS) states. The presence of two different spin states is attributed to the additional interactions of Cr(III) centers with adjacent siloxane bridges, which can lead to higher symmetries, thereby favoring the LS state. With the help of isotope labeling studies, we show that the observed LS Cr(III) species participate in ethylene polymerization.

## Results and Discussion

The silica-supported Cr(III) alkyl material **1-SiO<sub>2</sub>**, Cr[CH(SiMe<sub>3</sub>)<sub>2</sub>]<sub>3</sub>@SiO<sub>2-700</sub>, was prepared by contacting a bright green benzene solution of Cr[CH(SiMe<sub>3</sub>)<sub>2</sub>]<sub>3</sub> (**1**) with silica, partially dehydroxylated at 700 °C (SiO<sub>2-700</sub>; ca. 0.8 OH groups/nm<sup>2</sup>). This step, followed by washing and drying, yields a bright green solid **1-SiO<sub>2</sub>**. The IR spectrum of **1-SiO<sub>2</sub>** shows a decrease in the intensity of the band associated with surface OH groups and the concomitant appearance of the characteristic IR bands of alkyl ligands at ca. 3000 cm<sup>-1</sup> (Figure S1), consistent with grafting via protonolysis of the alkyl ligand. Notably, only a fraction of complex **1**, initially added in a 0.95:1 molar ratio with respect to the surface OH groups (0.26 mmol OH/g SiO<sub>2-700</sub>), reacts as evidenced by the presence of residual silanols in the IR spectrum. This partial grafting is likely due to the relatively large size of the molecular complex **1**. The elemental analysis shows a Cr loading of 0.29 wt. % and 0.99 wt. % of C, corresponding to 0.21 Cr/surface OH group and is consistent with the formation of mono-grafted (≡SiO)–Cr[CH(SiMe<sub>3</sub>)<sub>2</sub>]<sub>2</sub> surface sites, with an average of two alkyl ligands per grafted Cr center.

We then performed XAS in order to evaluate the oxidation state and local environment of the Cr surface sites in **1-SiO<sub>2</sub>**. The experimental XAS spectra on the Cr K-edge for the studied samples **1** and **1-SiO<sub>2</sub>** are shown in Figure 2a (see also Figure S2 for the details on data processing). The overall shapes of the normalized XAS spectra of the molecular and grafted compound are similar, thus indicating a related structure between the resulting surface species and compound **1**. The slightly higher edge energy of **1-SiO<sub>2</sub>** is consistent with the replacement of [CH(SiMe<sub>3</sub>)<sub>2</sub>] by surface siloxy ligands.<sup>[7]</sup>

The largest differences between the spectra of **1** and **1-SiO<sub>2</sub>** are observed in the two peaks in pre-edge and rising edge regions (see inset in Figure 2a), typical of Cr(III) species.<sup>[7,14]</sup> The features A and B, which can be attributed to the Cr d- and p<sub>z</sub> states respectively (see Figure S3), decrease in intensity and shift towards higher energies upon grafting. The broad pre-edge feature in **1-SiO<sub>2</sub>** centered at 5990 eV and consisting of two peaks is characteristic of Cr<sup>III</sup> ions with siloxide ligands.<sup>[7]</sup> The small intensity of features A and B suggests a change of geometry and possibly indicates additional coordination of adjacent siloxane bridges (≡Si–O–Si≡) to Cr (see Figure 1, bottom), as frequently observed for other silica-supported metal sites.<sup>[15]</sup> To address this complexity, we took advantage of the previously reported library of molecular Cr compounds to quantitatively evaluate the oxidation state and the number of alkyl bonds in the studied sample (see Supporting Information Section 2.2 for the details).<sup>[7]</sup> The library contains 23 experimental spectra of bulk and molecular references augmented with 39 theoretical spectra of surface-supported sites (see Figure S4). The references cover Cr(II–VI) charge states with different ligand types. The results obtained using a classical linear combination fit analysis can be found in the Supporting Information (Figure S5 and Table S2), while further discussion in the main text is based on a supervised

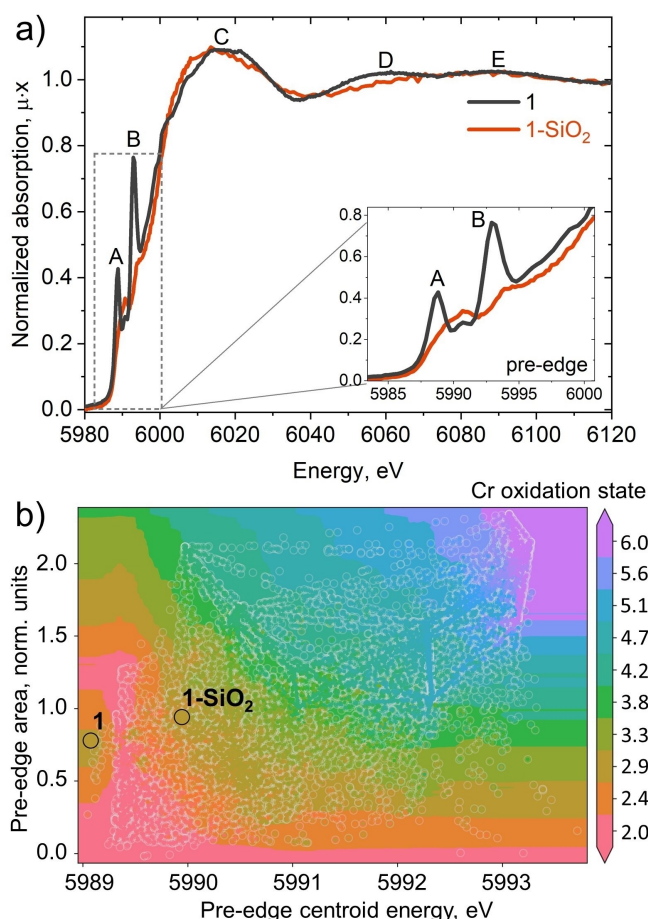


**Figure 2.** a) Experimental Cr K-edge XANES spectra for complex **1** before and after grafting on  $\text{SiO}_2\text{-700}$ . The inset shows the pre-edge energy region of the spectra. b) Classification of the Cr oxidation state for studied complexes based on the pre-edge centroid energy and area. The colored scatter plot refers to the pre-edge descriptors for the 10 000 linear combinations of spectra from the reference library.<sup>[7]</sup> The background color is the result of the oxidation state classification by the Extra Trees ML algorithm trained on the points from the scatter plots.

ML approach that utilized reference spectra as a training set. To address the heterogeneity of surface sites, we extended the library of spectra of pure species with their linear combinations and generated 10 000 mixtures. Several independent Extra Trees<sup>[16]</sup> models were trained on this extended library. The input features for each algorithm were either pre-edge descriptors (pre-edge area and centroid energy) or experimental data points on a uniform energy grid in the pre-edge region (5985–5997 eV) or near-edge region (5985–6100 eV). The regression task was solved for the output features “number of alkyl bonds” and “metal oxidation state”; these results are shown in Figure 2b and Table 1. Figure 2b combines a scatterplot for the pre-edge descriptors from the library of mixtures (colored points) and the results of the prediction of the ML algorithm trained on these descriptors (background color). The spectra of **1** and **1-SiO<sub>2</sub>** were projected on this map and overlap with the region of the Cr oxidation state 2.4–3.3. Note that **1** was part

**Table 1:** Prediction of the Cr oxidation state and number of alkyl bonds in **1-SiO<sub>2</sub>** using exclusively the pre-edge spectrum and the near-edge region of the spectrum but excluding pre-edge features.

	pre-edge 5985–5997 eV	near-edge 5985–6100 eV
Average Cr oxidation state	$3.2 \pm 0.3$	$3.2 \pm 0.2$
Number of alkyl bonds	1.7	1.4

of the library used in reference,<sup>[7]</sup> while **1-SiO<sub>2</sub>** was previously unseen by the algorithm. Table 1 shows the prediction of the Cr oxidation state and the number of alkyl bonds according to the ML algorithm trained on the spectral points. These results indicate that the surface species are mainly Cr(III) sites with ca. 1.4–1.7 alkyl ligands, in agreement with the elemental analysis data (C/Cr ratio of 14–15). They are also in agreement with the linear combination analysis predicting alkylated Cr(III) species to be the major component with admixture of surface species with siloxide bonds (Table S2). Finally, to further validate the hypothesis of additional interaction of Cr center to the silica surface, we compare the experimental spectrum of **1-SiO<sub>2</sub>** with theoretical calculations of DFT-optimized models of grafted species (Figure S3). The observed reduced intensity of shoulder B is consistent with a change of geometry to non-planar (quasi-tetrahedral) caused by additional interaction to siloxane bridges. The presence of a small fraction of bis-grafted sites, namely  $(\equiv\text{SiO})_2\text{-Cr}[\text{CH}(\text{SiMe}_3)_2]$ , cannot be excluded. Such species have already been proposed upon grafting **1** on silica, albeit partially dehydroxylated at a lower temperature.<sup>[12]</sup>

We next perform CW EPR spectroscopic studies of **1** and **1-SiO<sub>2</sub>** (Figure 3) in order to evaluate the electronic structure of the obtained Cr(III) species, associated with specific symmetry and spin states. The molecular complex **1** appeared to be in a pure high-spin (HS,  $S=3/2$ ) state at 5 K, as evidenced by its CW EPR spectrum (Figure 3, black): where a single  $S=3/2$  Cr(III) species with a purely axial symmetric zero-field splitting (ZFS) tensor ( $E/D=0$ ) is observed, consistent with previously reported data for Cr(III) HS complexes.<sup>[12,14,17]</sup> These results are in agreement with its ca.  $C_{3v}$  symmetry, strongly favoring the HS ( $S=3/2$ ) state. In contrast, **1-SiO<sub>2</sub>** contains both HS (100–250 mT) and low-spin (LS,  $S=1/2$ ; 300–400 mT) species, as evidenced by the two signals in the CW EPR spectrum (Figure 3, blue).

Simulation of the CW EPR spectrum of **1-SiO<sub>2</sub>** (Figure 3, red) reveals the presence of three sites: two  $S=3/2$  HS and one  $S=1/2$  LS species. The HS sites show ZFS tensor rhombicity parameters  $E/D$  (1) = 0.0858 and  $E/D$  (2) = 0.0082 (see Figure S8 for the individual simulations of each species) which suggests a similar geometry with **1**, with relative weighting factors 73.8% and 21.9%, respectively. The minor LS species (4.3%) probably differ in the local environment. Based on the combination of elemental analysis data and ML-assisted XAS, we suggest that the major HS fraction presents two alkyl ligands and therefore assign this species to a mono-grafted  $(\equiv\text{SiO})\text{-Cr}[\text{CH}(\text{SiMe}_3)_2]$ . We reason that the deviation from the purely



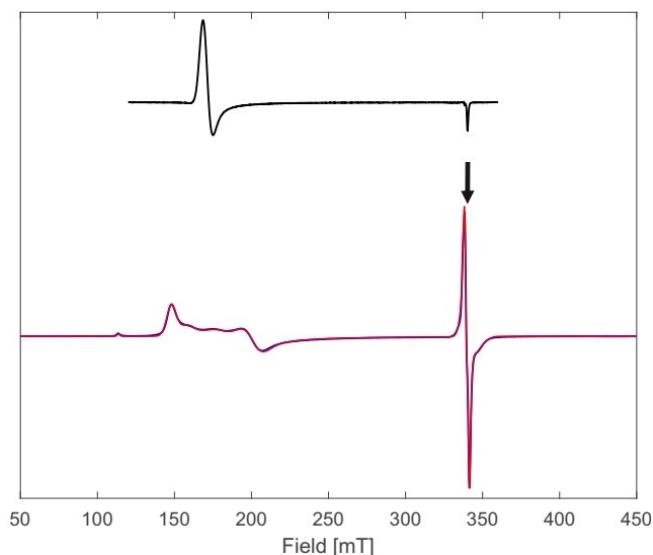
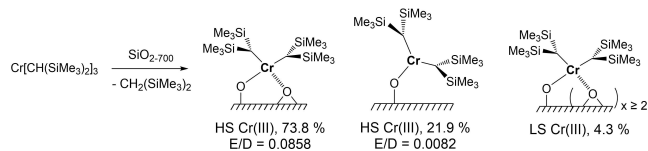


**Figure 3.** 9.5 GHz CW EPR spectra of **1** (black) and **1-SiO<sub>2</sub>** (blue), measured at 5 K, and simulation (red) of the two HS (weighting factors 73.8% and 21.9%) and LS (weighting factor 4.3%) Cr(III) species. The field position for the pulse EPR measurements (see below) is marked with a black arrow.

axial symmetry might be caused by additional interactions of the Cr center with the surface siloxane bridges ( $\equiv\text{Si}-\text{O}-\text{Si}\equiv$ , see Scheme 1), while the interaction with OH groups is less likely due to their low surface density (ca. 0.8 OH groups/nm<sup>2</sup>), especially after grafting.<sup>[15,18]</sup> This is also consistent with the changes in the pre-edge region observed in the XAS spectra (see Figure 2a). This assignment is in agreement with the  $S=3/2$  Cr(III) surface sites with only slightly larger rhombicity parameter ( $E/D=1/9$ ), previously observed as a major fraction (73.8%) within the material obtained upon the contact of **1** with a less dehydroxylated SiO<sub>2</sub> and assigned to mono-grafted sites.<sup>[12]</sup> The minor fraction of the HS Cr(III) species with  $E/D=0.0082$  (weighting factor 21.9%) has a lower ZFS tensor rhombicity, which suggests that its symmetry is closer to the axial compared to the major fraction. We therefore proposed that these species correspond to the mono-grafted sites showing a weaker interaction with the surrounding surface (see



**Scheme 1.** Tentative assignment of Cr surface sites after grafting of **1** on SiO<sub>2-700</sub> resulting in the presence of two mono-grafted HS and one LS site. While the major fraction of HS sites present one coordination to surface siloxane bridges, the LS sites present even additional coordination ( $x \geq 2$ ) to the surface, breaking the symmetry of the quasi-tetrahedral HS site and allowing the stabilization of a LS Cr(III) site. The relative ratios are estimated by the simulation of the CW EPR spectra of **1-SiO<sub>2</sub>**.

Scheme 1). Alternatively, it could correspond to a small fraction of bis-grafted species ( $\equiv\text{SiO})_2-\text{Cr}[\text{CH}(\text{SiMe}_3)_2]$ , even if typically not expected upon grafting on SiO<sub>2-700</sub>.

We then focused on the elucidation of the nature of the minor fraction of the observed Cr sites, namely the LS Cr species with  $g$  tensor principal values  $g=[2.0172 \pm 0.004; 2.0161 \pm 0.002; 2.0004 \pm 0.001]$  (weighting factor 4.3%; marked with a black arrow in Figure 3), a species that was not observed in the previous work.<sup>[12]</sup> The  $g$  tensor parameters indicate nearly axial symmetry. Such LS Cr surface sites could in principle be ascribed to either LS Cr(III) or Cr(V) sites.<sup>[12]</sup> Yet, these values are atypical for  $S=1/2$  Cr(V) species, where silica-supported Cr sites usually show a well-known value of  $g=1.974$ .<sup>[19]</sup> The presence of Cr(V) species in **1-SiO<sub>2</sub>** is also unlikely based on the XAS data. The measured  $g$  tensor parameters are in fact consistent with the typical range of silica-supported LS Cr(III) species.<sup>[9,20]</sup> At the same time, the question arises whether this minor fraction of Cr species is a mono-grafted or a bis-grafted Cr(III) site, similar to the previously observed ( $\equiv\text{SiO})_2-\text{Cr}[\text{CH}(\text{SiMe}_3)_2]$ .<sup>[12]</sup> In order to answer this question, we further characterized the local environment of this Cr(III) species with pulse EPR spectroscopy, namely 9.5 GHz HYSCORE, where the coupling between paramagnetic centers and close-by magnetic nuclei, such as <sup>1</sup>H of the  $[\text{CH}(\text{SiMe}_3)_2]$  ligands, can be observed.<sup>[21]</sup> We note that due to the extremely fast transverse relaxation rates of Cr(III) species,<sup>[21b,22]</sup> we have been able to perform hyperfine spectroscopy only for the LS species (Figure 3, marked with an arrow). For this species, we observed two distinct <sup>1</sup>H hyperfine couplings, together with a “matrix” <sup>29</sup>Si peak from the bulk SiO<sub>2</sub> (Figure 4a).

Assuming axially symmetric hyperfine coupling tensors (see Supporting Information Part 1 for details), the simulation of the experimental HYSCORE spectrum reveals two <sup>1</sup>H hyperfine couplings of  $a_{\text{iso}}(1)=4.5 \pm 0.5$  MHz,  $\mathbf{a}_{\text{dip}}(1)=[-3.5 \ -3.5 \ 7.0]$  MHz, and  $a_{\text{iso}}(2)=-39.0 \pm 0.5$  MHz,  $\mathbf{a}_{\text{dip}}(2)=[-3.75 \ -3.75 \ 7.5]$  MHz (Figure 4b). Using the point-dipole approximation,<sup>[23]</sup> the Cr–H distance for the first <sup>1</sup>H was estimated from  $\mathbf{a}_{\text{dip}}$  to be  $r_{\text{Cr-H}}(1)=2.81 \pm 0.15$  Å. While being slightly larger than the typically observed values for the corresponding molecular compounds, this distance is consistent with the reported metal– $\alpha$ -H distances in grafted complexes featuring  $[\text{CH}(\text{SiMe}_3)_2]$  ligands.<sup>[9,23b]</sup> For instance, the Cr–H distance for the related ( $\equiv\text{SiO})-\text{CrCp}[\text{CH}(\text{SiMe}_3)_2]$  site was estimated to be ca. 2.55 Å.<sup>[9]</sup> At the same time, the observed <sup>1</sup>H isotropic hyperfine couplings  $a_{\text{iso}}$  are in line with the values previously observed for the corresponding Cr(III),<sup>[9]</sup> as well as for Ti(III) alkyl complexes.<sup>[10,23b]</sup> The presence of two distinct hyperfine couplings indicates that there are two H atoms in close proximity to the Cr(III) center, consistent with two  $\alpha$ -H atoms of the  $[\text{CH}(\text{SiMe}_3)_2]$  ligands. Therefore, this minor LS Cr(III) species most likely presents two  $[\text{CH}(\text{SiMe}_3)_2]$  ligands, similar to the HS ( $\equiv\text{SiO})-\text{Cr}[\text{CH}(\text{SiMe}_3)_2]_2$  sites. The change in spin state however suggests a relevant change in its coordination environment and geometry. Taking this into account, we hypothesize that such change could arise from additional donor-acceptor interaction of Cr(III) center with oxygen surface atoms. Such interactions could again

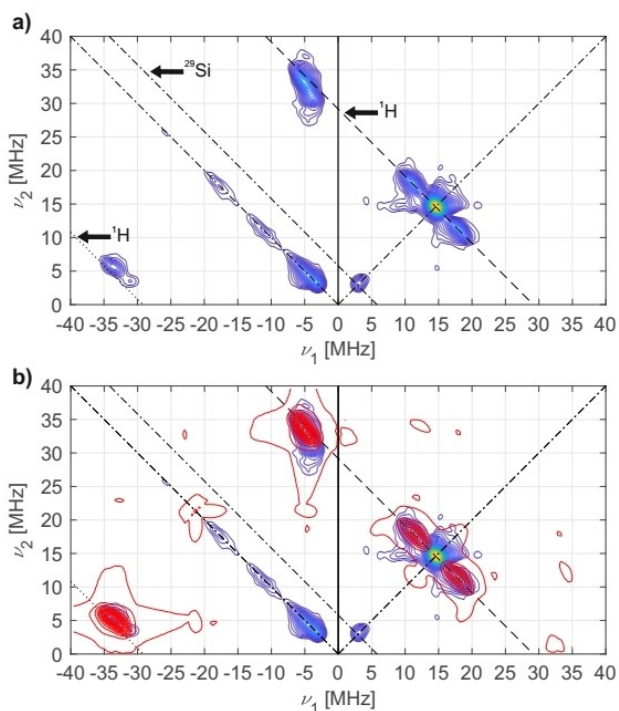


**Figure 4.** a) 9.5 GHz experimental HYSCORE spectrum of (blue to yellow) of **1-SiO<sub>2</sub>** measured at 3.8 K.  $^1\text{H}$  and  $^{29}\text{Si}$  nuclear frequencies are marked with the corresponding anti-diagonal lines. b) Simulation (red) of  $^1\text{H}$  hyperfine couplings observed in the experimental HYSCORE spectrum (blue to yellow).

arise with more nearby oxygen atoms in the surface siloxane bridges ( $\equiv\text{Si}-\text{O}-\text{Si}\equiv$ , see Scheme 1). Note that the change of Cr(III) alkyl  $[\text{CpCr}(\text{CH}(\text{SiMe}_3)_2)_2]$  spin state from HS to LS was previously associated with additional coordination of Cr(III) center to the nearby siloxane bridges.<sup>[9]</sup>

As previously reported,<sup>[11]</sup> **1-SiO<sub>2</sub>** is active in ethylene polymerization at room temperature without any induction period (see Figure S9). Its activity during the first minute upon contact with  $\text{C}_2\text{H}_4$  (10 bar) reaches ca. 1.6  $\text{kg}_{\text{PE}}(\text{mmol}_{\text{Cr}}\text{h})^{-1}$  and constantly decreases, reaching ca. 50  $\text{g}_{\text{PE}}(\text{mmol}_{\text{Cr}}\text{h})^{-1}$  after 1 h of polymerization. The produced PE is characterized by a high molecular weight ( $M_w=130\text{ kg mol}^{-1}$ ) and a large dispersity value ( $M_w/M_n=24.5$ , see section 2.4 and Table S3 in the Supporting Information for more details), consistent with previous observations.<sup>[11]</sup> The broader molecular weight distribution compared to the original Phillips catalyst ( $M_w/M_n=14.6$ ) was previously explained by the interactions between the Cr species and the various surface silanol ( $\equiv\text{Si}-\text{OH}$ ) or siloxane ( $\equiv\text{Si}-\text{O}-\text{Si}\equiv$ ) groups: different degrees of interaction with the surface were observed and resulted in different active sites.<sup>[11]</sup> This hypothesis is consistent with our XAS and EPR data, where various Cr(III) species are observed.

We then investigated the activity of the HS and LS Cr(III) sites on **1-SiO<sub>2</sub>**. The CW EPR features for both HS and LS species change upon contact with ethylene (see Figure 5a), providing evidence that both the HS and LS Cr(III) species change after exposure to  $\text{C}_2\text{H}_4$ . A similar

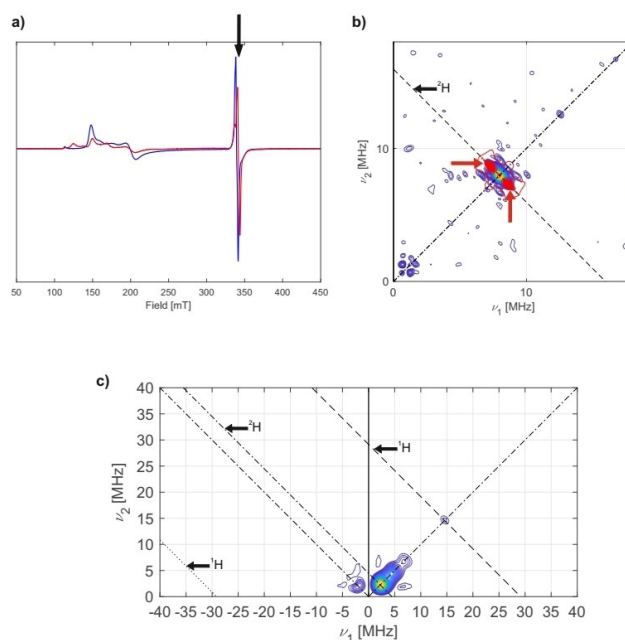


**Figure 5.** a) 9.5 GHz CW EPR spectra of **1-SiO<sub>2</sub>** before (blue) and after (red) contact with  $\text{C}_2\text{D}_4$ . b) 34.5 GHz HYSCORE spectrum of **1-SiO<sub>2</sub>** after contact with  $\text{C}_2\text{D}_4$  (blue to yellow), together with the simulation (red) of  $^1\text{H}$  hyperfine coupling (marked with red arrows). c) 9.5 GHz HYSCORE spectrum of **1-SiO<sub>2</sub>** after its contact with  $\text{C}_2\text{D}_4$ . Signal intensities of the 9.5 GHz HYSCORE spectra in Figure 5c are normalized to the signal intensities of the spectrum (Figure 4a) by the maximal modulation depths (see Supporting Information for further explanations).

change in the CW EPR spectra upon contact with  $\text{C}_2\text{H}_4$  has also been observed for the HS Cr(III) species obtained with less dehydroxylated silica.<sup>[12]</sup> In this case, the mono-grafted HS ( $\equiv\text{SiO}-\text{Cr}[\text{CH}(\text{SiMe}_3)_2]_2$ ) species were suggested to be active in ethylene oligomerization, while the active sites of ethylene polymerization were assigned to the bis-grafted ( $\equiv\text{SiO})_2\text{Cr}[\text{CH}(\text{SiMe}_3)_2]$  species, which we could not directly observe. In addition, these changes could be explained by the distortion in the coordination geometry caused by nearby polymer chains. Due to the considerable grafting density, the spectrum of an inactive site may be affected by polymers growing at neighboring active sites. While we cannot exclude that HS sites are active in ethylene polymerization, the activity of LS sites can be further studied by multifrequency pulse EPR experiments after contact with deuterium-labeled ethylene ( $\text{C}_2\text{D}_4$ ). Note that the  $g$  tensor symmetry for this species has changed to orthorhombic after the contact with  $\text{C}_2\text{D}_4$  (see Figure 5a, marked with arrow). This is consistent with modifications of the coordination environment, likely indicating a de-coordination or a weaker interaction of the Cr(III) center of ( $\equiv\text{Si}-\text{O}-\text{Si}\equiv$ )<sub>x</sub>( $\equiv\text{SiO})-\text{Cr}[\text{CH}(\text{SiMe}_3)_2]_2$  with surface siloxane bridges ( $\equiv\text{Si}-\text{O}-\text{Si}\equiv$ ) upon the interaction with ethylene.

The disappearance of both previously observed  $^1\text{H}$  signals in the 9.5 GHz HYSCORE spectrum after polymerization (see Figures 4a and 5c) indicates an increased distance between the magnetically coupled  $\alpha\text{-}^1\text{H}$  nuclei of

the ligands and the Cr center, consistent with the direct insertion of  $C_2D_4$  into the original Cr(III)–C bonds. This hypothesis is further supported by the appearance of  $^2H$  hyperfine couplings in the 34.5 GHz HSCORE spectrum (Figure 5b, marked with red arrows) with a magnitude of  $a_{iso}(^2H) = 1.5$  MHz ( $a_{dip} = [-0.8 \text{ } -0.8 \text{ } 1.6]$  MHz) (Figure 5b, red). Such ethylene insertion into the metal-carbon bond and chain growth is known as the Cossee-Arlman mechanism<sup>[24]</sup> and usually results in ultra-high molecular weight PE,<sup>[10]</sup> consistent with the high molecular weight of the obtained PE ( $M_w = 130 \text{ kg mol}^{-1}$ ). The same mechanism was previously observed for the Cr(III) alkyl species  $[CpCr(CH(SiMe_3)_2)_2]$ , also active in the production of PE with high molecular weight.<sup>[9]</sup> This mechanism is also reminiscent of the previously described “augmented” Cossee-Arlman mechanism of ethylene insertion into the Ti(III)–C bond of the active sites of the Ziegler–Natta catalysts and the well-defined surface-supported Ti(III) alkyl species.<sup>[10]</sup> This process was reported to involve delocalization of the unpaired electron density in the TS of ethylene insertion, combined with an increased  $\pi$ -character of the metal-carbon bonds. Indeed, an increased spin density on one of the  $^1H$  nuclei of the  $[CH(SiMe_3)_2]$  ligands, which reaches a magnitude of 39.0 MHz (see Figure 4b), suggests that there is a delocalization of unpaired electron density within the observed LS Cr(III) alkyl species. This is consistent with an interaction of the SOMO and one of the two degenerate  $\pi$ -orbitals of the  $[CH(SiMe_3)_2]$  fragment.

Therefore, the LS Cr(III)  $(\equiv Si-O-Si \equiv)_x (\equiv SiO)-Cr[CH(SiMe_3)_2]_2$  species in **1-SiO<sub>2</sub>**, are indeed active in ethylene polymerization. A change of its symmetry from axial to orthorhombic after contact with  $C_2H_4$  could be rationalized by the de-coordination to the surface  $(\equiv Si-O-Si \equiv)$  siloxane bridges upon polymerization. In this case, the  $SiO_{2-700}$  surface probably acts as a hemilabile ligand of the Cr(III) center; whose behavior is similar to the polymerization process on  $MgCl_2$ -surfaces for the Ti-based Ziegler–Natta catalysts as previously suggested.<sup>[10]</sup> Various degrees of interactions of the Cr center with nearby  $(\equiv Si-O-Si \equiv)$  groups (and growing polymer chains) could then explain the high polydispersity ( $M_w/M_n$ ) values of PE produced by **1-SiO<sub>2</sub>**.

While Cr alkyl species were considered to be the active sites of ethylene polymerization of the original Phillips catalyst, such species have not yet been directly characterized. The direct observation of ethylene insertion via the Cossee-Arlman mechanism for the silica-supported Cr(III) species  $(\equiv Si-O-Si \equiv)_x (\equiv SiO)-Cr[CH(SiMe_3)_2]_2$  indicates that similar species could indeed be the active sites of  $C_2H_4$  polymerization in the Phillips catalyst. Note that the LS Cr(III) alkyls are also identified as the active sites of ethylene polymerization for the  $CrCp[CH(SiMe_3)_2]@SiO_{2-700}$  system that was used to model the industrial Union Carbide catalyst.<sup>[9]</sup> Based on the similarity of the PE properties produced with the Phillips catalyst and **1-SiO<sub>2</sub>** systems,<sup>[11]</sup> the active sites of the Phillips catalyst could have a similar structure and spin state as this of the Cr(III)  $(\equiv Si-O-Si \equiv)_x$ - $(\equiv SiO)-Cr[CH(SiMe_3)_2]_2$  species. Such additional surface interactions, whose strength could vary from site to site,

could explain a high degree of dispersity, typical for the Phillips catalysts.

## Conclusion

We have prepared and characterized the molecularly well-defined heterogeneous Cr(III) ethylene polymerization catalyst  $Cr[CH(SiMe_3)_2]_3@SiO_{2-700}$  (**1-SiO<sub>2</sub>**), which has been proposed to be a model directly related to the widely used Phillips industrial catalysts.<sup>[10]</sup> Based on ML-supported XAS studies, we show that this material primarily contains Cr(III) species, which we assigned to Cr(III) silica-supported alkyls. We further show that the majority of the surface species are bis-alkyl Cr(III) sites,  $(\equiv SiO)-Cr[CH(SiMe_3)_2]_2$  with various degrees of interaction of the Cr(III) centers with nearby  $(\equiv Si-O-Si \equiv)$  groups. We propose that these additional surface interactions are responsible for the different observed spin states of Cr(III) centers (high-spin vs. low-spin), as well as for the production of polyethylene with high polydispersity. In particular, the observed LS Cr(III) alkyls  $(\equiv Si-O-Si \equiv)_x$ - $(\equiv SiO)-Cr[CH(SiMe_3)_2]_2$  are shown to be involved in ethylene polymerization, as evidenced by hyperfine EPR spectroscopy. The polymerization involves  $C_2H_4$  insertion into the Cr(III)–C bond that likely proceeds via an “augmented” Cossee-Arlman mechanism, as proposed for the similar Cr-based Union Carbide system,<sup>[9]</sup> as well as for well-defined Ti(III) alkyl catalysts<sup>[10]</sup> and heterogeneous Ziegler–Natta catalysts.<sup>[24]</sup> The similar PE produced with the Phillips catalyst and investigated **1-SiO<sub>2</sub>** systems suggests that the active sites of both materials present an akin structure and spin state. These results help us bridge the gap between the industrial and well-defined supported catalysts, opening ways for the design of highly active materials.

## Acknowledgements

We acknowledge Mr. Peter Kälin (Mikrolabor Service, ETH Zurich) for the elemental analysis. Dr. Romain Berthoud and Dr. John Severn are acknowledged for enabling HT-SEC measurements. A.A. is supported by an SNF–ANR grant (Mr. CAT 2–77275-15). A.N. and D.T. are grateful to the Swiss National Foundation (SNF) for financial support of this work (grant no. 200020B 192050 and 200021 169134, respectively). A.G. and S.G. acknowledge the financial support from the Ministry of Science and Higher Education of the Russian Federation (Agreement N° 075–15-2021-1363). O.V.S acknowledges the financial support of the Swiss State Secretariat for Education, Research and Innovation (SERI) Bilateral Science and Technology cooperation program.

## Conflict of Interest

The authors declare no conflict of interest.

## Data Availability Statement

The data that support the findings of this study are available from the corresponding author upon reasonable request.

**Keywords:** EPR Spectroscopy · Ethylene Polymerization · Heterogeneous Catalysis · Machine Learning · Surface Chemistry

- [1] N. Kashiwa, *J. Polym. Sci. Part A* **2004**, *42*, 1–8.
- [2] M. P. McDaniel, in *Advances in Catalysis*, Vol. 53 (Eds.: B. C. Gates, H. Knözinger), Academic Press, **2010**, pp. 123–606.
- [3] E. Groppo, G. A. Martino, A. Piovano, C. Barzan, *ACS Catal.* **2018**, *8*, 10846–10863.
- [4] E. Groppo, A. Damin, F. Bonino, A. Zecchina, S. Bordiga, C. Lamberti, *Chem. Mater.* **2005**, *17*, 2019–2027.
- [5] N. M. Peek, D. B. Jeffcoat, C. Moisii, L. van de Burgt, S. Profeta Jr., S. L. Scott, A. E. Stiegman, *J. Phys. Chem. C* **2018**, *122*, 4349–4358.
- [6] C. Brown, A. Lita, Y. Tao, N. Peek, M. Crosswhite, M. Mileham, J. Krzystek, R. Achey, R. Fu, J. K. Bindra, M. Polinski, Y. Wang, L. J. van de Burgt, D. Jeffcoat, S. Profeta, A. E. Stiegman, S. L. Scott, *ACS Catal.* **2017**, *7*, 7442–7455.
- [7] D. Trummer, K. Searles, A. Algasov, S. A. Guda, A. V. Soldatov, H. Ramanantoanina, O. V. Safonova, A. A. Guda, C. Copéret, *J. Am. Chem. Soc.* **2021**, *143*, 7326–7341.
- [8] a) M. P. Conley, M. F. Delley, G. Siddiqi, G. Lapadula, S. Norsic, V. Monteil, O. V. Safonova, C. Copéret, *Angew. Chem. Int. Ed.* **2014**, *53*, 1872–1876; b) M. F. Delley, C. S. Praveen, A. P. Borosy, F. Núñez-Zarur, A. Comas-Vives, C. Copéret, *J. Catal.* **2017**, *354*, 223–230; c) M. F. Delley, F. Núñez-Zarur, M. P. Conley, A. Comas-Vives, G. Siddiqi, S. Norsic, V. Monteil, O. V. Safonova, C. Copéret, *Proc. Natl. Acad. Sci. USA* **2014**, *111*, 11624–11629.
- [9] D. Trummer, A. G. Nobile, P.-A. Payard, A. Ashuiev, Y. Kakiuchi, D. Klose, G. Jeschke, C. Copéret, *Chem. Sci.* **2022**, *13*, 11091–11098.
- [10] A. Ashuiev, F. Allouche, N. Wili, K. Searles, D. Klose, C. Copéret, G. Jeschke, *Chem. Sci.* **2021**, *12*, 780–792.
- [11] H. Ikeda, T. Monoi, Y. Sasaki, *J. Polym. Sci. Part A* **2003**, *41*, 413–419.
- [12] G. A. Martino, A. Piovano, C. Barzan, Y.-K. Liao, E. Morra, K. Hirokane, M. Chiesa, T. Monoi, E. Groppo, *J. Catal.* **2021**, *394*, 131–141.
- [13] a) C. Copéret, A. Comas-Vives, M. P. Conley, D. P. Estes, A. Fedorov, V. Mougel, H. Nagae, F. Núñez-Zarur, P. A. Zhizhko, *Chem. Rev.* **2016**, *116*, 323–421; b) C. Copéret, F. Allouche, K. W. Chan, M. P. Conley, M. F. Delley, A. Fedorov, I. B. Moroz, V. Mougel, M. Pucino, K. Searles, K. Yamamoto, P. A. Zhizhko, *Angew. Chem. Int. Ed.* **2018**, *57*, 6398–6440.
- [14] R. Grauke, R. Schepper, J. Rabeah, R. Schoch, U. Bentrup, M. Bauer, A. Brückner, *ChemCatChem* **2020**, *12*, 1025–1035.
- [15] a) D. Gajan, C. Copéret, *New J. Chem.* **2011**, *35*, 2403–2408; b) M. Chabanas, A. Baudouin, C. Copéret, J.-M. Basset, W. Lukens, A. Lesage, S. Hediger, L. Emsley, *J. Am. Chem. Soc.* **2003**, *125*, 492–504; c) J. Corker, F. Lefebvre, C. Lécuyer, V. Dufaud, F. Quignard, A. Choplin, J. Evans, J.-M. Basset, *Science* **1996**, *271*, 966–969; d) S. Soignier, M. Taoufik, E. Le Roux, G. Saggio, C. Dablemont, A. Baudouin, F. Lefebvre, A. de Mallmann, J. Thivolle-Cazat, J.-M. Basset, G. Sunley, B. M. Maunders, *Organometallics* **2006**, *25*, 1569–1577; e) E. Le Roux, M. Chabanas, A. Baudouin, A. de Mallmann, C. Copéret, E. A. Quadrelli, J. Thivolle-Cazat, J.-M. Basset, W. Lukens, A. Lesage, L. Emsley, G. J. Sunley, *J. Am. Chem. Soc.* **2004**, *126*, 13391–13399.
- [16] P. Geurts, D. Ernst, L. Wehenkel, *Machine Learning* **2006**, *63*, 3–42.
- [17] J. Rabeah, M. Bauer, W. Baumann, A. E. C. McConnell, W. F. Gabrielli, P. B. Webb, D. Selent, A. Brückner, *ACS Catal.* **2013**, *3*, 95–102.
- [18] M. P. Conley, G. Lapadula, K. Sanders, D. Gajan, A. Lesage, I. del Rosal, L. Maron, W. W. Lukens, C. Copéret, R. A. Andersen, *J. Am. Chem. Soc.* **2016**, *138*, 3831–3843.
- [19] B. Cage, A. K. Hassan, L. Pardi, J. Krzystek, L.-C. Brunel, N. S. Dalal, *J. Magn. Reson.* **1997**, *124*, 495–498.
- [20] M. F. Delley, G. Lapadula, F. Núñez-Zarur, A. Comas-Vives, V. Kalendra, G. Jeschke, D. Baabe, M. D. Walter, A. J. Rossini, A. Lesage, L. Emsley, O. Maury, C. Copéret, *J. Am. Chem. Soc.* **2017**, *139*, 8855–8867.
- [21] a) P. Höfer, A. Grupp, H. Nebenführ, M. Mehring, *Chem. Phys. Lett.* **1986**, *132*, 279–282; b) N. A. Hirscher, C. H. Arnett, P. H. Oyala, T. Agapie, *Organometallics* **2020**, *39*, 4420–4429.
- [22] S. Chhabra, D. M. Smith, B. E. Bode, *Dalton Trans.* **2018**, *47*, 10473–10479.
- [23] a) A. Schweiger, G. Jeschke, *Principles of Pulse Electron Paramagnetic Resonance*, Oxford University Press, **2001**; b) F. Allouche, D. Klose, C. P. Gordon, A. Ashuiev, M. Wörle, V. Kalendra, V. Mougel, C. Copéret, G. Jeschke, *Angew. Chem. Int. Ed.* **2018**, *57*, 14533–14537.
- [24] E. J. Arlman, P. Cossee, *J. Catal.* **1964**, *3*, 99–104.

Manuscript received: September 8, 2023

Accepted manuscript online: November 16, 2023

Version of record online: November 29, 2023